INSTITUTE OF PHYSICS PUBLISHING JOURNAL OF PHYSICS D: APPLIED PHYSICS

J. Phys. D: Appl. Phys. **39** (2006) 5091–5096 doi:10.1088/0022-3727/39/23/029

Physicochemical characteristics of fluorine doped tin oxide films

A I Martínez[1,4], L Huerta[2], J M O-Rueda de León[3], D Acosta[3], O Malik[1] and M Aguilar[3]

[1] Electronics Department, National Institute for Astrophysics, Optics, and Electronics (INAOE), Luis E Erro No.1, 72000 Tonantzintla, Puebla, Mexico
[2] Instituto de Investigaciones en Materiales, Universidad Nacional Autónoma de México, AP 70-360, 04510 México DF, Mexico
[3] Institute of Physics, National Autonomous University of Mexico, 04510 Mexico DF, Mexico

E-mail: mtz.art@gmail.com

Received 29 August 2006
Published 17 November 2006
Online at stacks.iop.org/JPhysD/39/5091

Abstract

In this work, relationships between chemical and physical properties of fluorine doped tin oxide films prepared by the chemical spray pyrolysis technique have been studied. Changes in the structural, optical and electrical properties of these films in relation to their doping concentrations determined by the resonant nuclear reaction analysis and x-ray photoelectron spectroscopy (XPS) techniques have been correlated. By XPS measurements, it was found that the fluorine content in the tin oxide films does not induce any chemical shift of the Sn and O core levels. At the same time, XPS measurements are carried out at low binding energy, shown that the valence band of heavy doped tin oxide changes with respect to that determined in SnO_2 powder, due to the influence of the fluorine doping. In addition, it was shown that the formation of F–Sn complexes provides a decrease in both the concentration and mobility of the carriers.

(Some figures in this article are in colour only in the electronic version)

1. Introduction

It is well known that most oxides are insulators in amorphous or crystalline forms, particularly combinations between oxygen and silicon. However, some oxides exhibit metallic conduction; for example, vanadium oxide ($M_xV_2O_5$) and tungsten oxide (M_xWO_3) have a metal insulator transition at certain carrier concentration [1]. Other kinds of oxides with high conductivity are heavily doped n-type semiconductors such as In_2O_3 : Sn and SnO_2 : F known as ITO and FTO, respectively. Materials exhibiting simultaneously both high conductivity and optical transmittance are named transparent conductors; thin films of ITO and FTO fulfil these requirements; these materials are known as transparent conductor oxides (TCOs).

Investigations about TCOs are very comprehensive due to their great variety of applications [2]. Recently, many papers about properties of typical and new TCO materials with n- or p-type conductivity have been published [3–5]. Particularly, electrical and structural properties of undoped and fluorine doped tin oxide prepared by different techniques have been extensively studied [6-10]. However, studies of chemical analysis of impurities, e.g. fluorine in FTO, are few, because their low concentration is hard to detect by conventional techniques [11–15]. It has been reported that resonant nuclear reaction (RNR) analysis [12, 13] and secondary ion mass spectroscopy [14] techniques yield accurate chemical analysis for FTO films; in contrast, Auger electron spectroscopy and x-ray photoelectron spectroscopy (XPS) are not adequate to determine the fluorine content of FTO [10–13]. In addition, fluoride ions can be quantified with an ion chromatography technique after the etching of FTO films [15]. Despite this background, only a few works have studied the relationship between both chemical and physical properties of FTO films [10]. In this work, we will discuss the interplay between chemical and physical properties of FTO films prepared by the

[4] Author to whom any correspondece should be addressed.

Table 1. Characteristics of a selected group of FTO samples prepared from solutions of $SnCl_4$ with different concentrations of fluoride and similar thickness. The RMS values in brackets were determined from 2.5 μm × 2.5 μm AFM images; the others are from 5 μm × 5 μm AFM images. The concentration of F atoms was determined from the RNR depth profiles.

Sample series	F/Sn in solution	I_{200}/I_{110}	RMS roughness	F atoms/cm^{-3} × 10^{20}	n_e (cm^{-3}) ×10^{20}	μ (cm^2 V^{-1}s^{-1})
A	0.0	0.407	(7.03) 8.36	—	1.02	11.1
B	0.05	0.986	(6.93) 7.77	0.84–3.76	2.25	14.6
C	0.5	1.420	(11.9) 16.2	2.52–6.44	7.33	18.9
D	1.0	0.895	(22.4) 30.4	2.57–6.88	9.59	18.5
E	2.5	0.472	(17.6) 22.9	4.67–9.36	7.57	17.1
Powder	—	0.3	—	—	—	—

chemical spray pyrolysis (SP) technique using x-ray diffraction (XRD), atomic force microscopy (AFM), RNR, XPS, optical and Hall effect measurements.

2. Experimental procedure

The SP method grows TCO thin films at high deposition rates (∼200–500 nm min^{-1}) with optical and conducting properties comparable to other more expensive methods [16]. The design of different SP deposition apparatuses has focused on the control of substrate temperature (T_s) during the spraying process [16, 17] and the control of droplet size [18, 19]. However, some modifications have reduced the growth rate to very low values (∼6–30 nm min^{-1}) [18]. In this work, a SP technique controlled by a microprocessor without disturbing the high deposition rate was developed. All depositions were realized as follows: 20 ml of 0.2 M alcoholic solutions of $SnCl_4$ with different concentrations of NH_4F (at. ratio F/Sn = 0–2.5) were sprayed on glass or sapphire substrates; T_s was controlled at $T_s = 500 \pm 3\,^{\circ}$C. Some prepared samples were labelled as is indicated in table 1. In order to prepare films with different thicknesses 10 or 15 ml were sprayed for selected sample series. Sprayings were made using compressed air as carrier gas (5 psi) with a solution flow rate of 11 ml min^{-1} using a nozzle of stainless steel and a nozzle to substrate distance of 30 cm.

The film thickness was measured with an Alpha Step 200 profilometer. The electrical resistivity (ρ), Hall mobility (μ_H) and carrier concentration (n_e) were measured at room temperature using the van der Pauw method; Hall effect parameters were measured in a magnetic field of 0.2–0.3 T. The optical transmission (T) spectra of the films were obtained using air as reference. The structural characterization was carried out with an x-ray diffractometer operating in the Bragg–Brentano θ–θ geometry with Cu K_α radiation. A JSPM-5200 atomic force microscope was used to study the film surfaces. The chemical composition of the films was determined by both XPS and RNR techniques. The RNR is a qualitative analysis method that uses nuclear projectiles with energies near to the isolated resonance reaction of the element to be detected (fluorine); e.g. the nuclear reaction is $^{19}F(p, \alpha\gamma)^{16}O$ whose resonance lies at 340 keV [20]. It was produced with protons coming from a Van de Graaff accelerator with energies from 300 to 700 keV, detecting the γ-rays with a NaI (TI) scintillation device; for further details see [20]. The XPS chemical and valence band analysis was carried out in a UHV system of VG Microtech ESCA2000 Multilab, with an Al K_α x-ray source (1486.60 eV) and a CLAM4 MCD analyser. The surface of the samples was etched for 1 min with 3 kV Ar^+ at 0.11 μA mm^{-2}. The XPS spectrum was obtained at 55° of the normal surface with an energy step of 50 meV for high-resolution scans. The atomic relative sensitivity factor reported by Scofield was corrected by the transmission function of the analyser [21] and by the SnO_2 reference powder. The position of the signals was referenced to the background Ag $3d_{5/2}$ photopeak located at 367.81 eV, having a full-width half-maximum (FWHM) of 1.00 eV.

3. Results and discussion

3.1. Structural characterization and chemical analysis

The XRD measurements indicate that all deposited FTO films have the tetragonal rutile structure in polycrystalline configuration with a preferential grain orientation that depends on the fluoride concentration used in the solution. For example, more intense reflections of tin oxide powders are (1 1 0), (1 0 1) and (2 1 1), with an intensity ratio of the reflection (2 0 0) to the (1 1 0) of $I_{200}/I_{110} = 0.3$. Table 1 presents the I_{200}/I_{110} ratios of the deposited FTO films, showing higher values in B, C and D samples. Actually, the preferred orientation does not depend only on the precursor solutions; as is reported in tin oxide films prepared by chemical vapour deposition, it also depends on the film thickness [6]. Thus, samples C were prepared with different thicknesses. The I_{200}/I_{110} ratios were 1.93, 1.72 and 1.42 for films with thicknesses of 210 nm, 320 nm and 450 nm, respectively; thicker FTO films exhibit much less preferred orientation. In order to evaluate changes in this parameter at different fluoride concentrations, table 1 shows I_{200}/I_{110} ratios for films with similar thicknesses (450 ± 10 nm, only sample E exhibits a thickness of 410 nm). In addition, the mean size of the grains was determined using the classical Debye–Scherrer formula from the FWHM of the more intense reflections of the XRD patterns; the grain size values are between 30 and 50 nm.

Images of surface structure of the films in an area of 2.5 μm × 2.5 μm are shown in figure 1, it can be seen that the tin oxide surface (sample A) is smoother than those found in the FTO films. It is confirmed with the root mean square (RMS) roughness measurements carried out at different scanning areas. Table 1 shows the RMS roughness values coming from 2.5 μm × 2.5 μm images, the same behaviour has been found in 5 μm × 5 μm areas. The higher RMS roughness values were found at high fluoride concentration in the starting solution; it might be due to the formation of HF during the pyrolytical reaction, which etches the tin oxide surface promoting the development of granular structures shown in figure 1 (samples C, D and E). Also, at %F = 2.5 (sample

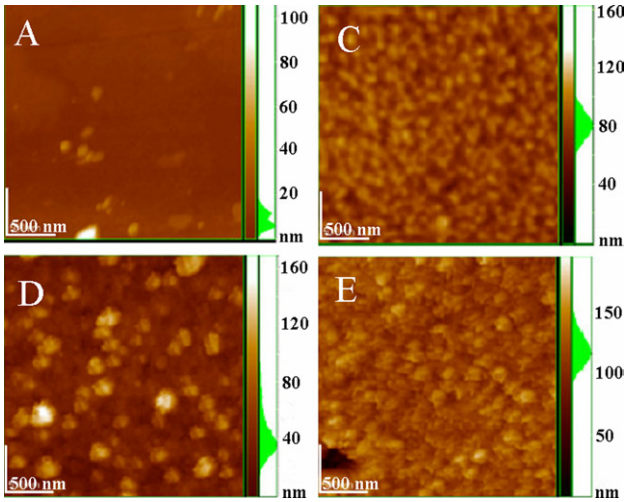

Figure 1. AFM images for samples A, C, D and E.

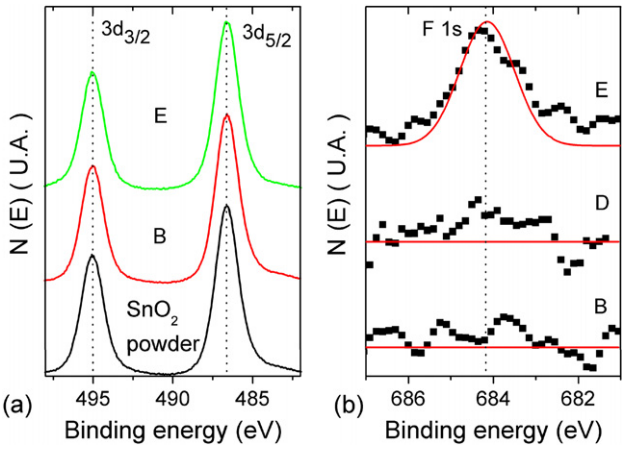

Figure 2. XPS spectra determined at different ranges: (*a*) the $3d_{3/2}$ and $3d_{5/2}$ orbitals for samples E and B compared with those from SnO_2 standard powder; no shift of these signals is demonstrated. (*b*) F 1s state for different FTO films.

E) some pits were observed. Moreover, from AFM images, changes in the size and shape of the particles can be observed; the particle size increases with the fluoride concentration but deceases at the highest fluoride concentration in the starting solution. Hence, the surface etching during the growth of the films is confirmed by both thickness measurements (lower film thickness in sample E) and from AFM images.

The XPS spectra of the non-ion bombarded FTO films revealed that tin, oxygen and carbon are present in the films. After the etch procedure of all the analysed tin oxide films, the signal corresponding to the contamination of hydrocarbon atoms decreases and signals corresponding to Sn $3d_{5/2}$, Sn $3d_{3/2}$ and O 1s were found at 486.60 eV, 495.02 eV and 530.44 eV, respectively (see figure 2(*a*)), these signals match very well with those reported for SnO_2 [22]. In addition, no chlorine signals were found at any depth in the analysed films due to its total evolution in the form of HCl. For FTO films prepared at low fluoride concentration, very weak peaks corresponding to fluorine are screened with the background noise (see figure 2(*b*), samples B and D). However, when the

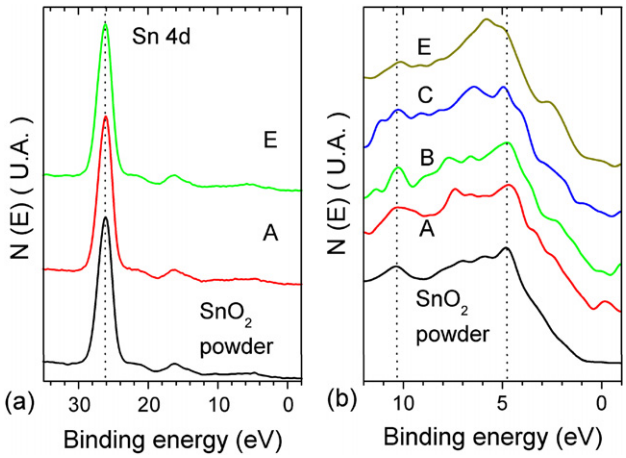

Figure 3. XPS spectra determined at low binding energies; (*a*) shows no shift of the Sn 4d state with respect to the standard SnO_2 powder. (*b*) Valence band spectra for different FTO films in comparison with that measured for SnO_2 powder.

fluoride content is very high in the starting solution (figure 2(*b*), sample E), a signal located at 684.4 eV was detected; this peak corresponds to the F 1s orbital [22]. Fluorine 1s signals by XPS studies have not been reported at this time for FTO films prepared by SP; for example, at very high fluoride concentration in the starting solution Amanullah *et al* [11] and Zhou *et al* [23] did not report F signals by XPS. Only for FTO films prepared by chemical vapour deposition [24] and by DC reactive sputtering [25], were F 1s signals observed; but these were assigned to C–F bonds arising from the precursors used [16]. In this work, F 1s signals can be assigned to the formation of Sn–F complexes formed in the SnO_2 framework. The atomic F/Sn ratio determined by XPS of the sample with greater fluorine content is 2% (sample E); in other samples, the F content is below the detection limit. No energy shift of the Sn and O core levels of FTO films with respect to SnO_2 powders was found (see figure 2(*a*)); it is in contrast to other works that report large shifts when F is present in tin oxide films [23]. As core level shifts are not adequate to evaluate the chemical role of fluorine in FTO films, XPS spectra at low energies (e.g. valence band—VB) were determined; these spectra reveal that the fluorine doping affects the shape of the VB; it is worth mentioning that this is the first work to measure VB of FTO films by XPS.

Figure 3 shows XPS spectra at low binding energy (E_b); (*a*) shows that the fluorine content in tin oxide films does not induce energy shift of the Sn 4d level with respect to that found in SnO_2 standard powder; thus even adding fluorine to the films, XPS measurements are not sensitive to orbital shifts. Figure 3(*b*) shows the VB-XPS spectra of FTO films compared with that from SnO_2 powder. For the SnO_2 powder, the determined VB spectrum shows very similar characteristics to those found by Cox *et al* [26] and Themlin *et al* [27], with prominent peaks located at $E_b = 4.8$ eV and 10.3 eV. The gradual appearance of a shoulder at E_b lower than 4.8 eV can be seen in figure 3(*b*) and prominent peaks keep the same location (4.8 and 10.3 eV). Nevertheless, at very high F content (sample E), the 4.8 eV peak becomes buried due to the appearance of the F 2p state at $E_b \sim 6$ eV; it confirms the formation of Sn–F complexes in this sample. Since there is no chemical shift

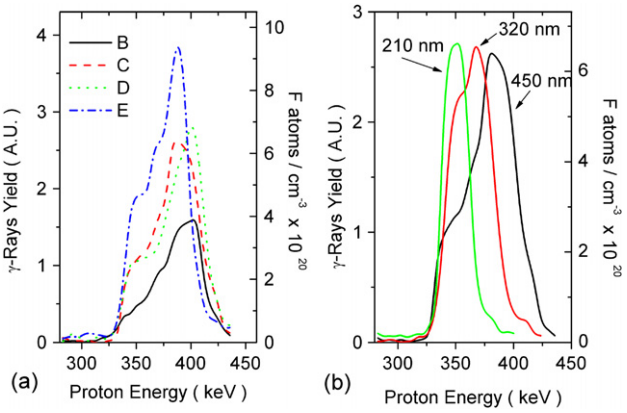

Figure 4. RNR depth profiles for: (*a*) FTO films with thickness of around 450 nm prepared with solutions with different fluoride concentration, (*b*) FTO samples series C prepared with different thicknesses. Observe that the proton energy is related to the sample thickness; for example, for thinner films the signal decay is shown at lower proton energies.

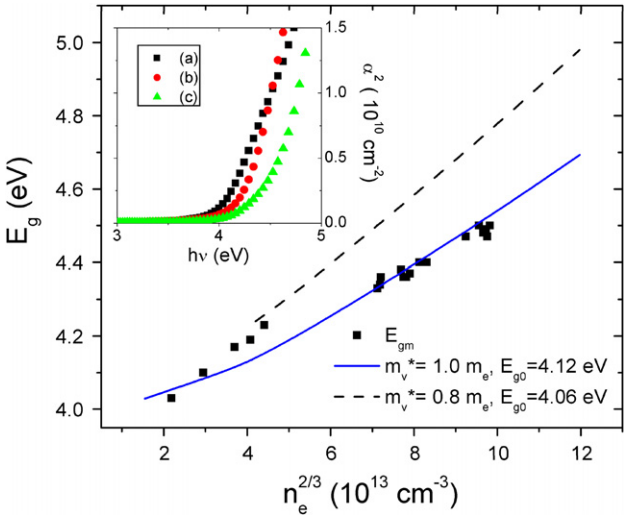

Figure 5. The measured band gap (E_{gm}) versus $n_e^{2/3}$ for FTO films. The lines represent the calculations from [29] for two different values of m_v^* with $m_c^* = 0.31m_e$. The inset shows the square of the absorption coefficient (α) versus the incident photon energy ($h\nu$) for FTO films with different carrier concentrations: (*a*) 1×10^{20} cm^{-3}, (*b*) 2.9×10^{20} cm^{-3} and (*c*) 9.6×10^{20} cm^{-3}.

in the Sn 4d state with respect to the F-doping level, in our experiments, changes in the VB spectra (the appearance of a shoulder at $E_b \sim 2.5$ eV) cannot be attributed to the formation of SnO, as was demonstrated by Themlin in SnO_2 layers on SnO [27]. The curve developed at ∼2.5 eV has been attributed to the Sn 5s state [27]; it forms the conduction band of SnO_2 but in SnO_2 : F, as in SnO, it becomes part of the VB.

The RNR consists of bombarding FTO films with protons of different energies, detecting the γ-rays produced by the nuclear reaction; the amount of γ-rays produced during the reaction is directly proportional to the fluorine content of the films and the proton energy used is proportional to the film thickness [20]. Therefore, with RNR measurements it is possible to obtain the fluorine depth profiles of the FTO films. Figure 4(*a*) shows depth profiles for FTO films prepared with different fluoride concentrations in the starting solution. From this figure, it can be observed that the F content near to the film surface (low energy part) is less than those found near to the interface film/substrate. For sample E, the incorporation of fluorine in the films is higher than those found in films prepared from other solutions. In addition, it can be observed, for films with F/Sn = 0.5–1.0 in the starting solution, that the incorporation of fluorine into films is slightly different. Figure 4(*b*) shows depth profiles for samples C with different thicknesses; it can be observed that the maximum of the profiles is almost the same for all samples C. However, thicker samples show less F content near the surface; this is due to the evolution of F from the surface during the film deposition, since thicker films exhibit more pronounced changes in the depth profiles than those presented in thinner films.

3.2. Optical and electrical measurements

The spectra of FTO films deposited on glass show that their transmittance is high ($T \geqslant 75\%$) over a large wavelength range (400–900 nm), spectra not shown. Because of the small energy gap of the glass substrate (∼3.5 eV), it is not possible to determinate the optical band gap of FTO films. The optical measurements of FTO films on sapphire were used to calculate the optical energy gap (E_{gm}) using the conventional method, which consists of extrapolating the linear part of $\alpha^2(h\nu)$ curves to $\alpha^2 = 0$ (see the inset of figure 5). Figure 5 shows that the optical band gap increases with the carrier concentration; as in different works [2, 28], this behaviour is attributable to the Moss–Burstein (MB) shift (conduction band filling), which is compensated by a band gap shrinkage, resulting as a net effect in an increment of E_{gm} with n_e. The band gap narrowing is a consequence of many-body interactions, which cause downward and upward shifts of the conduction and valence bands, respectively. The measured optical band gap, E_{gm}, can be expressed by

$$E_{gm} = E_{g0} + \Delta E_{gMB} - \Delta E_{gN}, \qquad (1)$$

where E_{g0} is the intrinsic band gap of SnO_2, ΔE_{gMB} is the MB shift and ΔE_{gN} is the contribution of the many-body interactions. For SnO_2 films, Sanon *et al* [29] calculated ΔE_{gN} by using the random phase approximation; ΔE_{gN} is an addition of the self-energies in the conduction and valence bands, which are due to the electron–electron (e–e) and electron–impurity (e–i) scattering effects. Figure 5 also shows the curves of equation (1) using the ΔE_{gN} values calculated by Sanon, for two different effective valence band mass (m_v^*) values taking an effective conduction band of $m_c^* = 0.31$, with $\Delta E_{gMB} = (3\pi^2 n_e)^{2/3}\hbar^2/2m_{vc}^*$. It can be seen in figure 5 that for high n_e values, the experimental data are well described with the calculations taking $m_v^* = 1.0m_e$ and $E_{g0} = 4.12$ eV; for low values of n_e, a little deviation can be observed; it may be due to the fact that m_c^* and m_v^* are not constant with n_e. As a comparison, Sanon *et al* found the best agreement between theory and experiments with $m_v^* = 1.0m_e$ and $E_{g0} = 4.18$ eV. The changes in the XPS-VB spectra of FTO films with the fluorine doping rules out the possibility of valence band bending variations with the carrier concentration, yielding changes in m_v^* with the doping. As can be observed in figure 5, the experimental data correlate well at low carrier

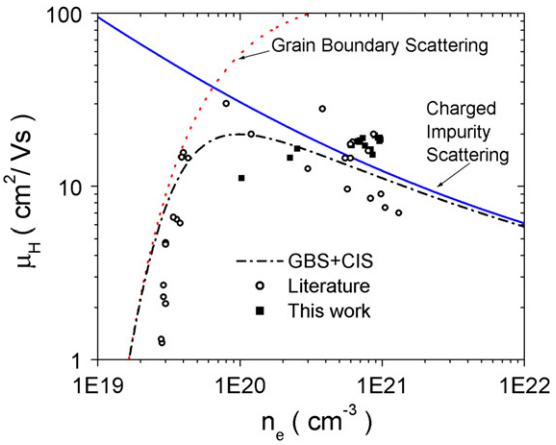

Figure 6. Calculated values of μ_H using the grain boundary (GBS) and the charged impurity (CIS) scattering mechanisms; also, a curve of the combined effects is included. Open circles indicate experimental values of n_e and μ_H reported in the literature for undoped and F-doped tin oxide films; filled squares indicate the values measured in this work.

concentrations with calculations with $m_v^* = 0.8m_e$, in contrast, for high values of n_e, the experimental data have a good agreement with $m_v^* = 1.0\,m_e$.

The effects of the fluorine doping can be observed with the increase in the carrier concentration in FTO films; for example, when the fluoride concentration in the starting solution increases, both the fluorine content in the films and n_e increase. However, the fluorine concentrations measured with the RNR technique are lower than those n_e values found by Hall measurements (see table); it confirms that the free carriers in FTO films comes from both oxygen vacancies and F-doping. In addition, when the fluoride content in the starting solution is very high (sample E), there is no correlation between the high fluorine content in films (detected with RNR and XPS techniques) and n_e. It might be due to the incorporation of fluorine atoms in the oxygen vacancies and to the formation of Sn–F complexes; this fact promotes a decrease in n_e and μ_H in sample E (see table 1) and changes in the valence band (figure 3(*b*)).

For samples C with different thicknesses, we found a decrease in ρ when the thickness increases; it is due to μ_H increases compensated by a decrement of n_e. Low values of n_e when the film thickness increase can be explained by using the RNR profiles presented in figure 4(*b*). When thicker films were prepared, the deposition time is longer; it promotes a high evolution of HF from the film and lower n_e values.

According to diverse carrier scattering mechanisms (CSMs), it has been found that in polycrystalline TCO films the main CSM is due to charged impurities (CI) and grain boundaries (GB) [30, 31]. The CI scattering was studied by Brooks and Herring (BH) [30], and the GB scattering was considered by Seto [31]. When different CSMs are present in semiconductors, the total mobility should be calculated with the Matthiensen rule; using it and the relations deduced by Seto and BH, it is possible to obtain a relationship between n_e and μ_H [4]. Figure 6 shows the total mobility taking into account both the grain boundary and the charged impurity scattering mechanisms in a graph of μ_H versus n_e. In this figure, it can be observed that the GB scattering mechanism play an important role only for $n_e \leqslant 1 \times 10^{20}\,\mathrm{cm}^{-3}$ and the CI scattering mechanism is more important for $n_e \geqslant 2 \times 10^{20}\,\mathrm{cm}^{-3}$; similar results have been reported by Minami and collaborators for ZnO films [4]. In addition, figure 6 includes both some experimental values found in the literature for tin oxide and FTO films and measured values obtained in this work for different FTO samples. Hence, the model used represents well the experimental values.

4. Conclusions

In this work, we have presented a discussion of the role of chemical analyses on the electrical properties of FTO thin films prepared by SP. It has been found that the fluorine content measured by the characterization methods in doped films does not match with those introduced in the starting solutions due to the evolution of the very stable HF sub-product. In addition, for the first time, the influence of fluorine doping on the valence band of tin oxide has been reported. It is shown that decrement of electrical properties of highly F-doped tin oxide is promoted by the formation of Sn–F complexes. Due to the variation of the VB shape with respect to the doping, and the lack of chemical shift of core levels, it can be ruled out that the VB is affected by the introduction of F atoms into the SnO_2 lattice.

Acknowledgments

The authors would like to thank J C Pineda, N Zuñiga, A Ortiz, R Hernandez and J G Morales for their valuable remarks and technical assistance.

References

[1] Crandall R S and Faughnan B W 1977 *Phys. Rev. Lett.* **39** 232
[2] Granqvist C G and Hultaker A 2002 *Thin Solid Films* **411** 1
[3] Choisnet J, Bizo L, Retoux R, Hebert S and Raveau B 2004 *J. Solid State Chem.* **177** 3748
[4] Minami T 2000 *MRS Bull.* **25** 38
[5] Kawazoe H, Yanagi H, Ueda K and Hosono H 2000 *MRS Bull.* **25** 28
[6] Kim K H and Chun J S 1986 *Thin Solid Films* **141** 287
[7] Demichelist F, Minetti-Mezzetti E, Smurro V, Tagliaferro A and Tresso E 1985 *J. Phys. D: Appl. Phys.* **18** 1825
[8] Bruneaux J, Cachet H, Froment M and Messad A 1991 *Thin Solid Films* **197** 129
[9] Messad A, Bruneaux J, Cachet H and Froment M 1994 *J. Mater. Sci.* **29** 5095
[10] Shanthi E, Banerjee A and Chopra K L 1982 *Thin Solid Films* **88** 93
[11] Amanullah F M, Pratap K J and Hari-Babu V 1998 *Mater. Sci. Eng. B* **52** 93
[12] Asomoza R, Maldonado A, Rickards J, Zironi E P, Farias M H, Cota-Araiza L and Soto G 1991 *Thin Solid Films* **203** 195
[13] Yueyuan X, Lennard W N and Akano N 1992 *Appl. Phys. Lett.* **60** 335
[14] Gottlieb B, Koropecki R, Arce R, Crisalle R and Ferron J 1991 *Thin Solid Films* **199** 13
[15] Nietering K E, Mason C F and Carter R O 1986 *Anal. Chim. Acta* **186** 279
[16] Bisht H, Eun H T, Mehrtens A and Aegerter M A 1999 *Thin Solid Films* **351** 109
[17] Martinez A I and Acosta D R 2005 *Thin Solid Films* **483** 107
[18] Paraguay F, Estrada W, Acosta D R, Andrade E and Miki-Yoshida M 1999 *Thin Solid Films* **350** 192

[19] Chopra K L, Major S and Pandya D K 1983 *Thin Solid Films* **102** 1
[20] De Lucio O G and Miranda J 1999 *J. Mexican Soc. Intrum.* **4** 12
[21] Scofield J H 1976 *J. Electron Spectrosc.* **8** 129
[22] NIST X-Ray Photoelectron Spectroscopy Database http://www.nist.gov/srd/nist20.htm
[23] Zhou Z B, Cui R Q, Hadi G M, Li W Y and Ding Z M 2001 *J. Mater. Sci.: Mater. Electron.* **12** 417
[24] Arefi-Khonsari F, Bauduin N, Donsanti F and Amouroux J 2003 *Thin Solid Films* **427** 208
[25] Martel A, Caballero-Briones F, Bartola-Perez P, Iribarren A, Castro-Rodriguez R, Zapata-Navarro A and Peña J L 2001 *Surf. Coat. Technol.* **148** 103
[26] Cox P A, Egdell R G, Hardin C, Patterson W R and Tavener P J 1982 *Surf. Sci.* **123** 179
[27] Themlin J M, Chtaib M, Henrard L, Lambin P, Darville J and Guilles J M 1992 *Phys. Rev.* B **46** 2460
[28] Hamberg I and Granqvist C G 1986 *J. Appl. Phys.* **60** R123
[29] Sanon G, Rup R and Mansingh A 1991 *Phys. Rev.* B **44** 5672
[30] Thangaraju B 2002 *Thin Solid Films* **402** 71
[31] Seto J Y W 1975 *J. Appl. Phys.* **46** 5247